PAPER

Mixed-ligand hydroxocopper(II)/pyridazine clusters embedded into 3D framework lattices†

Anna S. Degtyarenko,[a] Marcel Handke,[b] Karl W. Krämer,[c] Shi-Xia Liu,*[c] Silvio Decurtins,[c] Eduard B. Rusanov,[d] Laurence K. Thompson,[e] Harald Krautscheid[b] and Konstantin V. Domasevitch*[a]

Rational combination of pyridazine, hydroxo and carboxylate bridging ligands led to the assembly of three types of mixed-ligand polynuclear Cu(II) clusters (**A**: [Cu$_2$(µ-OH)(µ-pdz)(µ-COO)]; **B**: [Cu$_4$(µ$_3$-OH)$_2$(µ-pdz)$_2$]; **C**: [Cu$_5$(µ-OH)$_2$(µ-pdz)$_4$(µ-COO)$_2$(µ-H$_2$O)$_2$]) and their integration into 3D framework structures. Mixed-ligand complexes [Cu$_2$(µ-OH){TMA}(L)(H$_2$O)] (**1**), [Cu$_4$(µ$_3$-OH)$_2${ATC}$_2$(L)$_2$(H$_2$O)$_2$]·H$_2$O (**2**) [Cu$_4$(µ$_3$-OH)$_2${TDC}$_3$(L)$_2$(H$_2$O)$_2$]·7H$_2$O (**3**) (L = 1,3-bis(pyridazin-4-yl)adamantane; TMA^{3-} = benzene-1,3,5-tricarboxylate, ATC^{3-} = adamantane-1,3,5-tricarboxylate, TDC^{2-} = 2,5-thiophenedicarboxylate) and [Cu$_5$(µ-OH)$_2${X}$_4$(L)$_2$(H$_2$O)$_2$]·nH$_2$O (X = benzene-1,3-dicarboxylate, BDC^{2-}, n = 5 (**4**) and 5-hydroxy-benzene-1,3-dicarboxylate, HO-BDC^{2-}, n = 6 (**5**)) are prepared under hydrothermal conditions. Trigonal bridges TMA^{3-} and ATC^{3-} generate planar Cu(II)/carboxylate subtopologies further pillared into 3D frameworks (**1**: binodal 3,5-coordinated, doubly interpenetrated **tcj**-3,5-Ccc2; **2**: binodal 3,8-coordinated **tfz**-d) by bitopic pyridazine ligands. Unprecedented triple bridges in **1** (cluster of type **A**) support short Cu···Cu separations of 3.0746(6) Å. The framework in **3** is a primitive cubic net (**pcu**) with multiple bis-pyridazine and TDC^{2-} links between the tetranuclear nodes of type **B**. Compounds **4** and **5** adopt uninodal ten-coordinated framework topologies (**bct**) embedding unprecedented centrosymmetric open-chain pentanuclear clusters of type **C** with two kinds of multiple bridges, Cu(µ-OH)(µ-pdz)$_2$Cu and Cu(µ-COO)(µ-H$_2$O)Cu (Cu···Cu distances are 3.175 and 3.324 Å, respectively). Magnetic coupling phenomena were detected for every type of cluster by susceptibility measurements of **1**, **3** and **4**. For binuclear clusters **A** in **1**, the intracluster antiferromagnetic exchange interactions lead to a diamagnetic ground state (J = −17.5 cm^{-1}; g = 2.1). Strong antiferromagnetic coupling is relevant also for type **B**, which consequently results in a diamagnetic ground state (J_1 = −110 cm^{-1}; J_2 = −228 cm^{-1}, g = 2.07). For pentanuclear clusters of type **C** in **4**, the exchange model is based on a strongly antiferromagnetically coupled central linear trinuclear Cu$_3$ group (J_1 = −125 cm^{-1}) and two outer Cu centers weakly antiferromagnetically coupled to the terminal Cu ions of the triad (J_2 = −12.5 cm^{-1}).

Introduction

The study of metal–organic framework (MOF) structures adopted by linkage of polynuclear metal ion clusters is a special topic in coordination and materials chemistry and crystal engineering, and has attracted rapidly growing interest during the last decade.[1] In view of framework topologies,[2] the design of such solids offers a particularly successful approach. It allows to avoid the common limitations for the node connections imposed by the typical coordination numbers,[3] and therefore a diversity of extremely highly-connected frameworks became accessible by propagation of coordination geometries established by polynuclear clusters.[4] An even more important aspect considers the utility of the latter for functionalization of the MOFs towards specific applications in magnetism and catalysis,[5] while imprinting the inherent properties of the

[a]Inorganic Chemistry Department, Taras Shevchenko National University of Kyiv, Volodimirska Street 64/13, Kyiv 01601, Ukraine. E-mail: dk@univ.kiev.ua
[b]Institut für Anorganische Chemie, Universität Leipzig, Johannisallee 29, D-04103 Leipzig, Germany
[c]Departement für Chemie und Biochemie, Universität Bern, Freiestrasse 3, CH-3012 Bern, Switzerland. E-mail: liu@iac.unibe.ch
[d]Institute of Organic Chemistry, Murmanskaya Str. 4, Kyiv 253660, Ukraine
[e]Department of Chemistry, Memorial University of Newfoundland, St. John'sA1B 3X7, Canada

†Electronic supplementary information (ESI) available: Details for organic synthesis and characterization; IR spectra, TGA and thermo-XRPD patterns; X-ray structure refinement. CCDC 967343–967348. For ESI and crystallographic data in CIF or other electronic format see DOI: 10.1039/c4dt00174e

Table 1 Bridging coordination of non-chelating pyridazines towards Cu(II) ions[a]

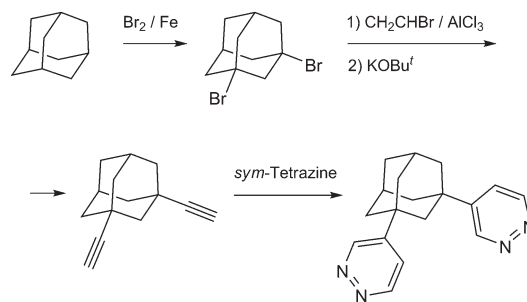| Complex	co-Bridge(s)	Cu···Cu/Å	Structural pattern and magnetic features	Ref.
$[Cu(OH)(sac)(\mu\text{-pdz})]_n$	μ-OH, μ-sac-N,O	3.360	1D chain of triply bridged Cu^{2+} ions; strong AFM, μ_{eff} (RT) = 0.99 μ_B	22
$[Cu(\mu\text{-pdz})Cl_2]_n$	μ-Cl (×2)	3.378	1D chain of triply bridged Cu^{2+} ions; μ_{eff} (RT) = 1.5–1.7 μ_B; low-temperature AF coupling	20a, 23
$[Cu(OH)(\mu\text{-pdz})(NO_3)]_n$	μ-OH, μ-NO$_3$-O,O'	3.322	1D chain of triply bridged Cu^{2+} ions; strong AFM, μ_{eff} (RT) = 1.08 μ_B	19
$[Cu_3(\mu\text{-pdz})_4(pdz)_2(\mu\text{-NO}_3)_2(NO_3)_4]$	μ-NO$_3$-O,O	3.406	Triple bridges $[M(\mu\text{-pdz})_2(\mu\text{-NO}_3)M]$; Discrete trinuclear; strong AFM, μ_{eff} (RT) = 1.51 μ_B	15, 19
$[Cu_3(OH)_2(\mu\text{-bpdz})_3(H_2O)_2\{CF_3CO_2\}_2]^{2+}$	μ-OH	3.236	Discrete trinuclear, triple bridges $[M(\mu\text{-pdz})_2(\mu\text{-OH})M]$	13
$[Cu(OH)(pp)](H_2NSO_3)\cdot H_2O$	μ-OH	3.394	1D chain of triply bridged Cu^{2+} ions	14a
$[Cu_2(OH)\{TMA\}(L)(H_2O)]$	μ-OH, μ-RCO$_2$-O,O'	3.075	Discrete binuclear cluster with triply bridged Cu^{2+} ions	This work
$[Cu_4(OH)_2\{ATC\}_2(L)_2(H_2O)_2]\cdot H_2O$	μ_3-OH	3.272	Discrete tetranuclear cluster	This work
$[Cu_4(OH)_2\{TDC\}_3(L)_2(H_2O)_2]\cdot 7H_2O$	μ_3-OH	3.334	The same	This work
$[Cu_5(OH)_2\{BDC\}_4(L)_2(H_2O)_2]\cdot 5H_2O$	μ-OH	3.175	Discrete pentanuclear cluster with a trinuclear triply-bridged skeleton $M\{(\mu\text{-pdz})_2(\mu\text{-OH})M\}_2$	This work
$[Cu_5(OH)_2\{HO\text{-BDC}\}_4(L)_2(H_2O)_2]\cdot 6H_2O$	μ-OH	3.187	The same	This work

[a] sac = saccharinate; bpdz = 4,4'-bipyridazine; pp = pyridazino[4,5-d]pyridazine; L = 1,3-bis(pyridazin-4-yl)adamantane; BDC = isophthalate; HO-BDC = 5-hydroxyisophthalate; TDC = thiophene-2,5-dicarboxylate; TMA = benzene-1,3,5-tricarboxylate; ATC = adamantane-1,3,5-tricarboxylate.

clusters into the extended lattices.[6] Therefore, the development of polynucleating ligand systems, which combine the abilities for generation of polynuclear fragments[7] and their further integration into the framework, has received a special value.[8]

Different types of azole and azine 1,2-dinitrogen donors are applicable to assemble clusters of variable nuclearity and establish pathways for magnetic exchange between paramagnetic metal ions, *cf.* copper(II) and cobalt(II). In this series, the pyridazine linker is a particular paradigm, while offering a large magnetic superexchange interaction and thus mediating magnetic exchange most efficiently in comparison with corresponding phthalazine, 1,2,4-triazole, 1,2,4-triazolate and pyrazolate analogs.[9] The ability of pyridazine to generate polynuclear complexes with tunable spin states of the metal ions is also known.[10] The attractiveness of polypyridazinyl ligands, however, was limited until now because of their low chemical accessibility. Actually, the preparative chemistry involving pyridazine relies on only one general method which is applicable for facile functionalization of different substrates, namely a very simple click reaction[11] involving inverse electron demand cycloadditions of 1,2,4,5-tetrazine.[12] Recent developments have made this key intermediate readily available,[12,13] thus offering flexible pathways towards pyridazine ligands.[13,14] A second potential drawback one might find is the inherent coordination ability of pyridazine.[13–16] It manifests a pronounced affinity towards d^{10} Cu(I) and Ag(I) ions, commonly generating either single, double or triple bridges between the metallic centres involved in the desired and peculiar polynuclear and polymeric motifs.[14,17] In the case of divalent d-metal ions, bridging coordination of this electron deficient and low basic ligand (pK_a = 2.24 for pyridazine *vs.* pK_a = 5.25 for pyridine) is less characteristic and predictable, compared with a simple monodentate pyridine-like function.[15,18] Nevertheless, double coordination of pyridazine may be stabilized using suitable complementary short-distance co-bridges, such

as hydroxo,[10,13,19] halogenido,[20] nitrato,[15] isothiocyanato,[10,21] and saccharinato,[22] and actually all of the reports for pyridazine bridges between 3d-metal ions consider such a multiple heteroligand linkage, which is best illustrated by a Cu(II) series (Table 1). Thus a promising approach towards the development of nanosized molecular magnets may rely on a synergism of the ligands in multicomponent systems[24] based upon bifunctional pyridazines, which could be well suited for the synthesis of extended frameworks incorporating polynuclear cluster units.

In this work we report the construction of unprecedented discrete di-, tetra- and pentanuclear copper(II)/pyridazine clusters and their integration into the 3D MOFs structures by the concerted action of representative di- and tricarboxylate linkers (H$_2$BDC = isophthalic acid; H$_2$HO-BDC = 5-hydroxyisophthalic acid; H$_2$TDC = thiophene-2,5-dicarboxylic acid; H$_3$TMA = trimesic acid; H$_3$ATC = adamantane-1,3,5-tricarboxylic acid) and prototypical pyridazine tecton 1,3-bis(pyridazin-4-yl)adamantane (L) (Scheme 1), which features a double ligand functionality established at a rigid alicyclic molecular platform.

Scheme 1 Synthesis of the bis-pyridazine ligand by a stepwise functionalization of the adamantane core.
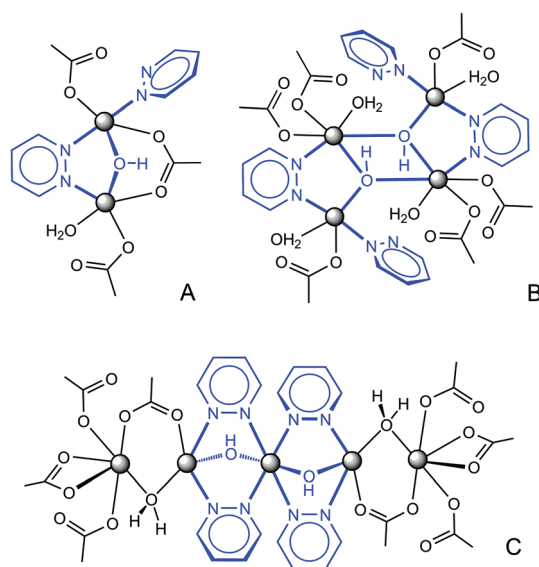
Results and discussion

Structure of the coordination compounds

All the compounds adopt 3D framework structures based upon multinuclear heteroligand clusters, which represent topological net nodes and thus provide a primary factor for the complicated connectivities. Three types of the observed clusters, such as binuclear in **1**, tetranuclear in **2**, **3** and pentanuclear units in **4** and **5** (Scheme 2), originate from a combination of three kinds of ligand bridges (pyridazine, hydroxo and carboxylate), while preserving a common simple submotif in the form of Cu ions linked by a double pdz/OH bridge. This suggests perfect compatibility of μ-pdz and μ-OH linkers, which are commonly concomitant and act in a synergetic manner.[10,13,19] In fact, the significance of the hydroxo bridges is most crucial for the present systems since the bidentate coordination of pyridazine itself is less applicable for the chemistry of transition metal dications, as stated above. In this view, the clusters demonstrate a clear structural hierarchy, which implies a basic hydroxocopper(II) core, pyridazine co-bridges, auxiliary carboxylate ligands and additional monodentate pyridazine and aqua

donors. The function of the carboxylate is most important for compounds **4** and **5**, providing expansion of the trinuclear $[Cu_3(\mu\text{-pdz})_4(\mu\text{-OH})_2]$ skeleton to a pentanuclear architecture. Especially close structural relationships may be found for binuclear (**A**) and tetranuclear (**B**) motifs. Doubling the cluster nuclearity is made possible by elimination of the carboxylate bridge and a simple dimerization along the Cu–OH sides with formation of two edge-sharing $[Cu_3(\mu_3\text{-OH})]$ fragments. Such a "dimer", often encountered for different combinations of bridging ligands, is particularly characteristic of the hydroxocopper systems.[25] Further intercluster connection with generation of frameworks occurs by the interplay of bipyridazine (as a bitopic linker between the clusters, establishing three or four Cu–N bonds) and dicarboxylate bridges (TDC^{2-} (**3**), BDC^{2-} (**4**), HO-BDC^{2-} (**5**)), which are equally important in view of the resulting topologies. This is contrary to the tricarboxylate (TMA^{3-} (**1**), ATC^{3-} (**2**)) frameworks. Trifunctional anions, as the three-coordinated nodes, provide an additional origin of connectivity and generate distinct planar Cu-carboxylate subtopologies, further pillared with bitopic bipyridazine ligands (Table 2).

A simpler binuclear cluster **A** was observed in $[Cu_2(\mu\text{-OH})\{TMA\}(L)(H_2O)]$ (**1**), with an unprecedented mixed-ligand pdz/OH/carboxylate triple bridge connecting two Cu ions at very short distances of Cu1···Cu2A 3.0746(6) Å and Cu1···Cu2B 3.1270(7) Å (for two orientations of the disordered fragment). The environments of metal ions are complete with monodentate carboxylate and pyridazine groups and aqua ligands (Fig. 1, Table 3). As was indicated by the values of Addison τ parameters,[26] the geometries of the coordination polyhedra are intermediate between idealized trigonal-bipyramidal ($\tau = 1$) and square-pyramidal ($\tau = 0$) extremes: for orientation A, $\tau = 0.66$ (Cu1) and 0.39 (Cu2A); for orientation B, $\tau = 0.53$ (Cu1) and 0.32 (Cu2B).

The low nuclearity of the cluster is likely a consequence of topology limitations imposed by the rigid trigonal triple-charged TMA^{3-} connector: the planar Cu/carboxylate subtopology in the form of a hexagonal net (Fig. 1b) clearly implies a three-fold coordination of the hydroxocopper nodes and their complementary charge of +3 [e.g. $Cu_2(\mu\text{-OH})$]. The bipyridazine ligands are accommodated on both axial sides of this plane, and they connect pairs of clusters at a distance of 13.56 Å and expand the structure in a third dimension as pillars between the successive hexagonal layers. The result is a rare binodal three- and five-connected $\{6^3\}\{6^9\cdot8\}$ net (three-letter notation is
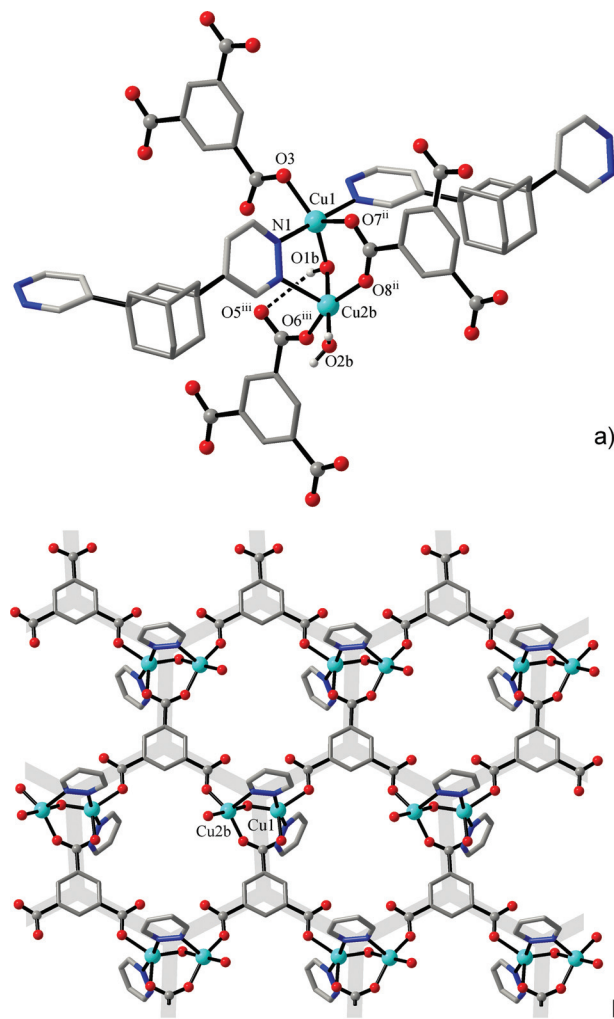

Scheme 2 Three kinds of polynuclear Cu/OH/pyridazine clusters, representing the structures of the reported complexes: **A** – binuclear motif in **1**; **B** – tetranuclear clusters in **2** and **3**; **C** – pentanuclear units in **4** and **5**, with a central trinuclear hydroxo/pyridazine core.

Table 2 Highly-connected topologies of MOFs **1–5**

Complex	Cluster type	Ligand coordination	Dimensionality	Net nodes (coordination)	Schläfli symbol	Topological type
1	**A**	3	2D → 3D^a	$[Cu_2(\mu\text{-OH})]$ (5), TMA (3)	$\{6^3\}\{6^9\cdot8\}$	**tcj**-3,5-Ccc2
2	**B**	3	2D → 3D^a	$[Cu_4(\mu_3\text{-OH})_2]$ (8), ATC (3)	$\{4^3\}_2\{4^6\cdot6^{18}\cdot8^4\}$	**tfz**-d (UO$_3$)
3	**B**	3	3D	$[Cu_4(\mu_3\text{-OH})_2]$ (6)	$\{4^{12}\cdot6^3\}$	**pcu** (α-Po)
4	**C**	4	3D	$[Cu_5(\mu\text{-OH})_2]$ (10)	$\{3^{12}\cdot4^{28}\cdot5^5\}$	**bct**
5	**C**	4	3D	$[Cu_5(\mu\text{-OH})_2]$ (10)	$\{3^{12}\cdot4^{28}\cdot5^5\}$	**bct**

^{a} Dimensionality of the Cu/carboxylate subtopology and the overall dimensionality of the resulting heteroligand frameworks.

Fig. 1 (a) Binuclear cluster in the environment of carboxylate and pyridazine ligands in the structure of **1**; (b) 2D Cu/carboxylate subtopology in the form of hexagonal net, with the pyridazine-N donors accommodated at two sides of the plane. Only one orientation of the disordered cluster is shown.
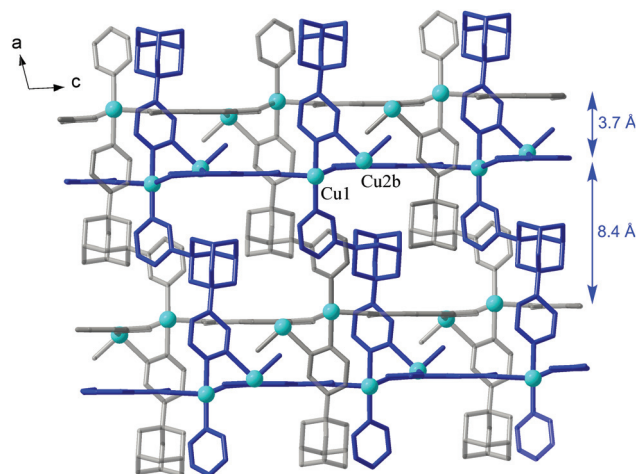
Table 3 Selected bond distances (Å) and angles (°) for [Cu$_2$(μ-OH)-{TMA}(L)(H$_2$O)] (**1**)[a]

Cu1–O3	2.0418(18)	O3–Cu1–N1	89.10(8)
Cu1–N4^i	2.043(2)	O3–Cu1–O7^{ii}	115.76(8)
Cu1–N1	2.053(2)	N4^i–Cu1–O7^{ii}	89.91(9)
Cu1–O7^{ii}	2.1577(16)	N1–Cu1–O7^{ii}	84.24(7)
		O3–Cu1–N4^i	91.75(9)
		N4^i–Cu1–N1	173.85(9)

Disordered fragment			
Orientation A		*Orientation B*	
Cu1–O1A	1.873(3)	Cu1–O1B	1.913(3)
Cu2A–O1A	1.906(3)	Cu2B–O1B	1.895(4)
Cu2A–O5^{iii}	1.946(2)	Cu2B–O6^{iii}	1.9264(19)
Cu2A–O4	1.984(2)	Cu2B–O8^{ii}	1.9307(18)
Cu2A–O2A	1.991(3)	Cu2B–O2B	1.952(4)
Cu2A–N2A	2.207(4)	Cu2B–N2B	2.262(4)
O1A–Cu1–N4^i	91.62(12)	O1B–Cu1–N4^i	86.79(12)
O1A–Cu1–N1	93.80(12)	O1B–Cu1–N1	96.27(12)
O1A–Cu2A–O5^{iii}	87.56(13)	O1B–Cu2B–O6^{iii}	88.57(13)
O1A–Cu2A–O4	88.78(14)	O1B–Cu2B–O8^{ii}	91.98(12)
O5^{iii}–Cu2A–O4	155.29(11)	O6^{iii}–Cu2B–O8^{ii}	159.17(9)
O1A–Cu2A–O2A	178.92(17)	O1B–Cu2B–O2B	178.52(14)
O1A–Cu2A–N2A	88.73(14)	O1B–Cu2B–N2B	87.98(15)
O5^{iii}–Cu2A–N2A	109.02(13)	O6^{iii}–Cu2B–N2B	104.15(12)
O4–Cu2A–N2A	95.32(13)	O8^{ii}–Cu2B–N2B	96.68(12)
Cu2A–O1A–Cu1	108.89(16)	Cu2B–O1B–Cu1	110.43(16)

[a] Symmetry codes: (i) −0.5 + x, −0.5 + y, z; (ii) x, −y, 0.5 + z; (iii) x, 1 − y, 0.5 + z.

Fig. 2 Interpenetration of two inversion-related 3D frameworks (marked with blue and grey bonds) in the structure of **1**. The hydroxo-copper-carboxylate layers are orthogonal to the drawing plane.

tcj-3,5-Ccc2), which appears to be very open and, therefore, two identical nets interpenetrate (Fig. 2). That is a class IIa interpenetration, Z = 2, with a full symmetry element 1̄.[27,28]

A comparable morphology of the framework is observed for the aliphatic analog of trimesic acid, 1,3,5-adamantanetricarboxylate (ATC$^{3−}$) in [Cu$_4$(μ$_3$-OH)$_2${ATC}$_2$(L)$_2$(H$_2$O)$_2$]·H$_2$O (**2**). That is a first coordination polymer generated by this ligand and we introduce ATC$^{3−}$ as a novel geometrically rigid tripodal linker, potentially complementing and expanding the chemistry of functional frameworks based upon TMA$^{3−}$ (such as HKUST-1).[29] Both metal ions adopt typical Jahn–Teller polyhedra in the form of square pyramids (Cu1; Addison parameter[26] τ = 0.18) or axially elongated octahedra (Cu2) (Table 4), with pyridazine-N donors positioned at the equatorial planes. In the metal–carboxylate subtopology, the net nodes exist as the above six-connected tetranuclear clusters [Cu$_4$(μ$_3$-OH)$_2$] and three-connected ATC$^{3−}$ (in 1 : 2 proportion), giving rise to a 2D

structure of the CdI$_2$ or Mg(OH)$_2$ type (Kagomé dual net, {4^3}$_2${4^6·6^6·8^3}, three-letter notation "**kgd**") (Fig. 3). Pairs of bipyridazine ligands, as double links, interconnect the clusters from the successive layers (separated at 12.83 Å), yielding a 3D eight- and three-coordinated framework, with a Schläfli point symbol {4^3}$_2${4^6·6^{18}·8^4} (**tfz**-d, topological type of UO$_3$) (Table 2). There are a limited number of structural precedents for such a linkage, most of which also incorporate polynuclear cluster nodes and trigonal TMA$^{3−}$ links.[30]
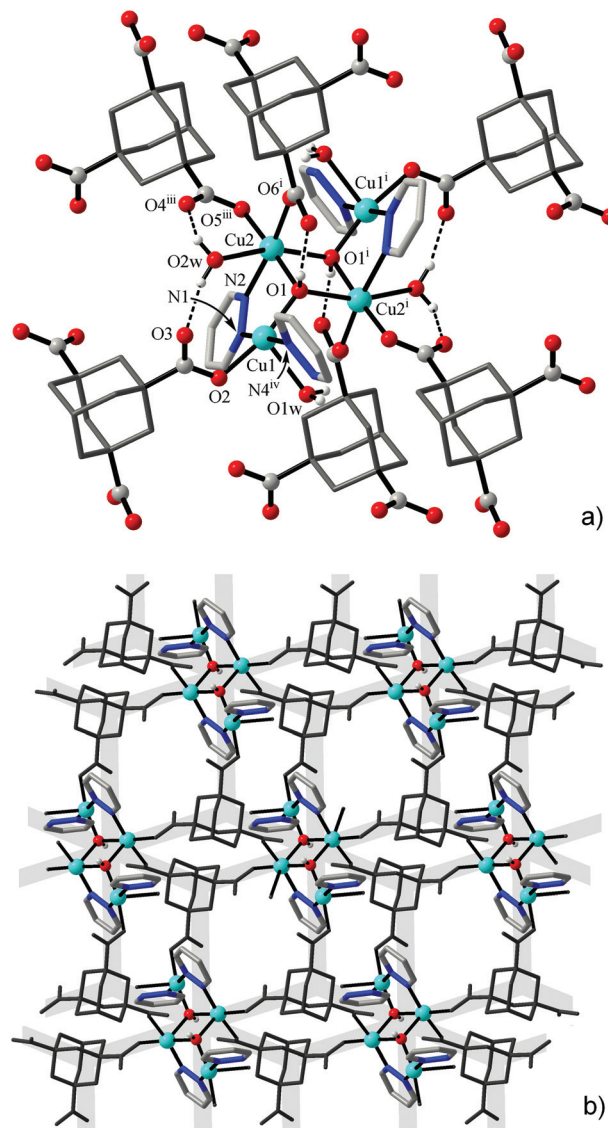
Table 4 Selected bond distances (Å) and angles (°) for tetranuclear complexes **2** and **3**[a]

$[Cu_4(\mu_3\text{-OH})_2\{ATC\}_2(L)_2(H_2O)_2]\cdot H_2O$ (**2**)

Cu1–O1	1.931(2)	Cu2–O6[ii]	1.948(3)
Cu1–O2	1.952(3)	Cu2–O5[iii]	1.953(3)
Cu1–N4[iv]	2.026(3)	Cu2–O1	1.962(2)
Cu1–N1	2.068(3)	Cu2–N2	2.016(3)
Cu1–O1w	2.359(3)	Cu2–O1[i]	2.423(2)
O1–Cu1–O2	167.55(11)	O6[ii]–Cu2–O5[iii]	85.36(12)
O1–Cu1–N4[iv]	94.38(12)	O6[ii]–Cu2–O1	97.84(11)
O2–Cu1–N4[iv]	93.50(12)	O5[iii]–Cu2–O1	176.64(12)
O1–Cu1–N1	86.13(12)	O6[ii]–Cu2–N2	173.27(12)
O2–Cu1–N1	86.29(12)	O5[iii]–Cu2–N2	90.36(12)
N4[iv]–Cu1–N1	178.20(13)	O1–Cu2–N2	86.36(12)
O1–Cu1–O1w	100.77(10)	O6[ii]–Cu2–O1[i]	99.00(10)
N4[iv]–Cu1–O1w	90.72(12)	O1–Cu2–O1[i]	85.52(10)
N1–Cu1–O1w	87.49(11)	N2–Cu2–O1[i]	86.53(11)
Cu1–O1–Cu2	114.38(12)	Cu2–O1–Cu2[i]	94.48(10)
Cu1–O1–Cu2[i]	120.24(12)		

$[Cu_4(\mu_3\text{-OH})_2\{TDC\}_3(L)_2(H_2O)_2]\cdot 7H_2O$ (**3**)

Cu1–O1[i]	1.920(2)	Cu2–O1	1.919(2)
Cu1–O1[i]	2.352(2)	Cu2–O6	1.968(2)
Cu1–O2	1.942(11)	Cu2–N4[iii]	2.007(3)
Cu1–O8[ii]	1.952(2)	Cu2–N2	2.058(3)
Cu1–O5[iv]	1.959(12)	Cu2–O10	2.236(2)
Cu1–N1	2.052(3)		
O1–Cu1–O2	160.6(3)	O1–Cu2–O6	172.67(10)
O1–Cu1–O8[ii]	97.53(10)	O1–Cu2–N4[iii]	91.96(10)
O2–Cu1–O8[ii]	84.5(4)	O6–Cu2–N4[iii]	87.77(11)
O1–Cu1–N1	88.00(10)	O1–Cu2–N2	88.41(10)
O2–Cu1–N1	90.8(4)	O6–Cu2–N2	89.29(10)
O8[ii]–Cu1–N1	174.25(11)	N4[iii]–Cu2–N2	159.51(12)
O5[iv]–Cu1–N1	83.1(3)	O1–Cu2–O10	93.71(9)
O1–Cu1–O1[i]	85.37(9)	O6–Cu2–O10	93.25(10)
N1–Cu1–O1[i]	94.72(10)	N2–Cu2–O10	90.06(10)
Cu1–O1–Cu1[i]	94.63(9)	Cu2–O1–Cu1[i]	110.79(10)
Cu2–O1–Cu1	120.57(12)		

[a] Symmetry codes for **2**: (i) −x, 2 − y, 1 − z; (ii) −1 + x, y, z; (iii) 1 − x, 1 − y, 1 − z; (iv) x, y, −1 + z. For **3**: (i) 1 − x, 2 − y, −z; (ii) −0.5 + x, 2.5 − y, −0.5 + z; (iii) 1.5 − x, 0.5 + y, 0.5 − z; (iv) −x, 2 − y, −z.

Fig. 3 (a) Tetranuclear cluster in **2** showing the hydrogen bonding interactions with μ₃-OH and aqua ligands; (b) Cu/carboxylate topology in the form of six- and three-connected CdI₂-like network. Note the intrinsic topological significance of the tricarboxylate linker. Symmetry codes: (i) −x, 2 − y, 1 − z; (ii) −1 + x, y, z; (iii) 1 − x, 1 − y, 1 − z; (iv) x, y, −1 + z.
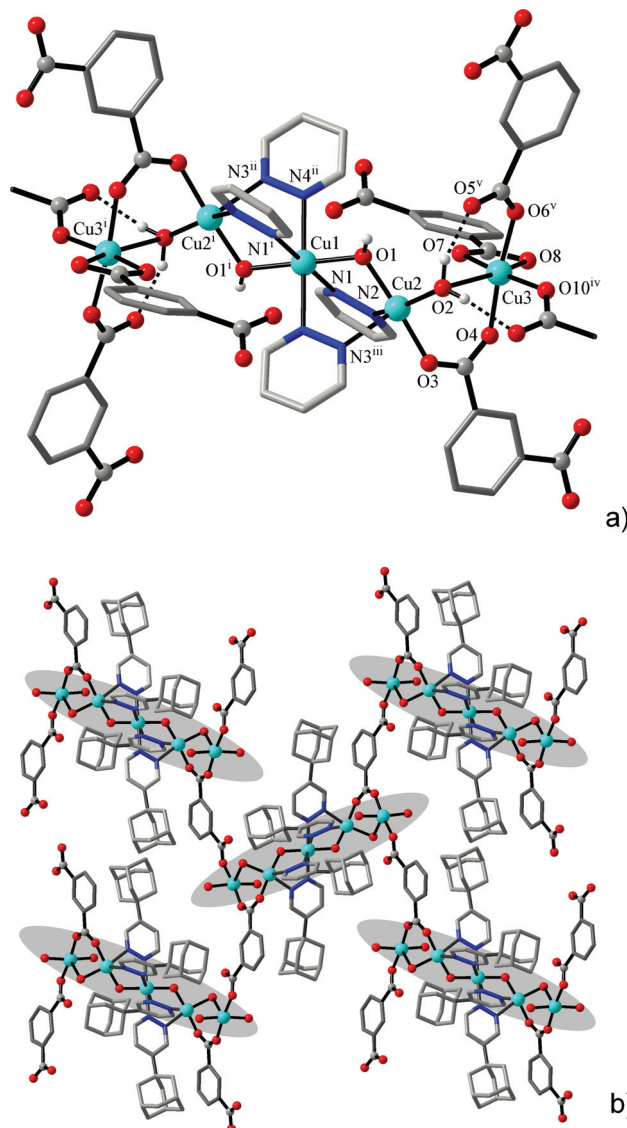
Similar tetranuclear net nodes are also observed for $[Cu_4(\mu_3\text{-OH})_2\{TDC\}_3(L)_2(H_2O)_2]\cdot 7H_2O$ (**3**). However, substitution of the carboxylate portion of the structure for dibasic thiophene-dicarboxylate leads to simplification of the entire array. This concerns the elimination of three-connected nodes and an increased carboxylate/cluster ratio (3 : 1), which in effect increases the dimensionality of the carboxylate subconnectivity, existing in the form of a primitive cubic net (**pcu**, Schläfli point symbol $\{4^{12}\cdot 6^3\}$). The bipyridazine bridges did not generate additional intercluster links, but rather repeat the existing links already established by the TDC²⁻ bridges. In this way, four out of six topological links are doubled as a result of the concerted action of both sorts of ligands (Fig. 4). Two Cu^II ions adopt square-pyramidal environments (Addison parameters[26] τ are 0.23 for Cu1 and 0.22 for Cu2) (Table 4).

The structures of the two isotypic compounds, $[Cu_5(\mu\text{-OH})_2\{X\}_4(L)_2(H_2O)_2]\cdot nH_2O$ (**4**: X = BDC²⁻, n = 5; **5**: X = HO-BDC²⁻, n = 6), are more complicated and they include pentanuclear net nodes (Fig. 4). The present open-chain centrosymmetric Cu₅ units are unprecedented yet comprising a central trinuclear core $[Cu_3(\mu\text{-OH})_2(pdz)_4]$ built up with two triple bis-pyridazino/hydroxo bridges, which itself is known for copper(II)[13] and cobalt(II)[10] pyridazine complexes. These units are extended to the pentanuclear pattern by connecting two Cu3 ions as annexes through carboxylate bridges and distal aqua ligands (Fig. 5). These outer ions have a typically distorted [4 + 2] octahedral coordination, whereas the environment geometry of Cu2 is close to a square pyramid with N3 in the apex position, with Addison parameters[26] τ = 0.41 (**4a** at 296 K), τ = 0.37 (**4b** at 105 K) and τ = 0.42 (**5**) (Table 5).

Fig. 4 (a) Primitive cubic framework of **3** viewed down the *b* direction showing interconnection of heteroligand carboxylate/pyridazine planes by additional carboxylate linkers. (b) The heteroligand planes with double organic bridges between the tetranuclear clusters constituting the framework nodes.

Fig. 5 (a) Pentanuclear centrosymmetric clusters observed in **4** and **5**. Note the compressed octahedral geometry around the Cu1 ion. (b) Mode of interconnection of the clusters by dicarboxylate links. Symmetry codes: (i) −*x*, −*y*, 2 − *z*; (ii) 0.5 − *x*, 0.5 + *y*, 2.5 − *z*; (iii) −0.5 + *x*, −0.5 − *y*, −0.5 + *z*; (iv) −1 + *x*, *y*, *z*; (v) −0.5 − *x*, 0.5 + *y*, 2.5 − *z*.

The most striking features of the local coordination geometries are the appreciably compressed octahedral environments adopted by the central Cu1 ions lying on the centre of inversion. For both of the compounds, these involve two pairs of long "equatorial" Cu–N bonds (2.1733(18)–2.300(2) Å) accompanied by two very short "axial" Cu–O1 bonds (1.901(2)–1.9086(16) Å). The only documented example of the $[Cu\{(\mu\text{-OH})\text{-}(\mu\text{-pdz})_2Cu\}_2]$ pattern, in a 4,4′-bipyridazine complex, also implies such a kind of coordination octahedron adopted by the central Cu ion (Cu–O 1.887(2); Cu–N 2.146(2)–2.340(3) Å).[13] Although these observations are suggestive of Jahn–Teller compression (indicating the unusual $\{d(z^2)\}$ electronic ground state of Cu1 ions), the present geometries, most likely, may be attributed to the dynamic disorder of an axis of Jahn–Teller elongation and consequent librational effects.[31] First, the examination of complex **4** at different temperatures (**4a**: 296 K, **4b**: 105 K, using the same single crystal) reveals an appreciable temperature dependence of the Cu1–N bond lengths. Being actually equivalent at r.t. (2.221(2) × 2 and 2.252(2) × 2 Å), two pairs of bonds became essentially differentiated upon cooling

(2.1733(18) × 2 and 2.300(2) × 2 Å) (Table 5). Second, mean-square displacement amplitude (MSDA)[32] analysis clearly indicates the presence of librational disorder involving all four Cu1–N bonds, at both temperatures (for Cu1–O1, Cu1–N1 and Cu1–N4 bonds, $<d^2>$ (×10⁴ Å²) = 11(11), 95(12) and 78(12) at 296 K, and 9(8), 74(11) and 41(10) at 105 K, respectively), with the corresponding $<d^2>$ values being particularly high at r.t. Importantly, the bonds adopted by Cu2 and Cu3 ions are actually temperature invariant (Table 5). The application of such an approach towards "compressed" coordination geometry of Cu^{2+} ions was extensively discussed by Halcrow.[31]

The fact that the cluster units accommodate in total eight carboxylate and four pyridazine groups allows a very high, up to twelve, connectivity at the net nodes.[4] The latter is

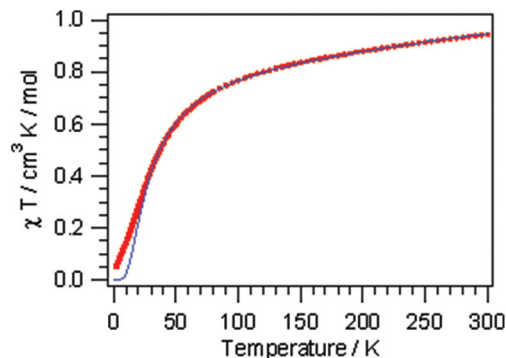**Table 5** Selected bond distances (Å) and angles (°) for pentanuclear complexes 4 and 5[a]

$[Cu_5(\mu\text{-}OH)_2\{BDC\}_4(L)_2(H_2O)_2]\cdot 5H_2O$ (**4a**, 296 K)

Cu1–O1	1.9086(16) × 2	Cu3–O10^{iv}	1.9085(17)
Cu1–N1	2.221(2) × 2	Cu3–O6^{v}	1.9593(19)
Cu1–N4	2.252(2) × 2	Cu3–O7	1.9614(16)
		Cu3–O4	1.9685(18)
Cu2–O1	1.8800(17)	Cu3–O8	2.482(2)
Cu2–O3	1.9286(18)	Cu3–O2	2.733(2)
Cu2–O2	2.0040(18)		
Cu2–N2	2.195(2)		
Cu2–N3^{iii}	2.224(2)		

$[Cu_5(\mu\text{-}OH)_2\{BDC\}_4(L)_2(H_2O)_2]\cdot 5H_2O$ (**4b**, 105 K)

Cu1–O1	1.9162(15) × 2	Cu3–O10^{iv}	1.9139(16)
Cu1–N1	2.300(2) × 2	Cu3–O6^{v}	1.9616(16)
Cu1–N4	2.1733(18) × 2	Cu3–O7	1.9615(14)
		Cu3–O4	1.9715(16)
Cu2–O1	1.8784(15)	Cu3–O8	2.4799(18)
Cu2–O3	1.9245(15)	Cu3–O2	2.7019(18)
Cu2–O2	2.0093(16)		
Cu2–N2	2.1671(19)		
Cu2–N3^{iii}	2.227(2)		

$[Cu_5(\mu\text{-}OH)_2\{HO\text{-}BDC\}_4(L)_2(H_2O)_2]\cdot 6H_2O$ (**5**)

Cu1–O1	1.901(2) × 2	Cu3–O8	1.915(2)
Cu1–N1	2.138(3) × 2	Cu3–O6^{iv}	1.927(2)
Cu1–N4	2.344(3) × 2	Cu3–O4	1.949(2)
		Cu3–O10^{v}	1.964(2)
Cu2–O1	1.882(2)	Cu3–O11^{v}	2.541(3)
Cu2–O3	1.933(2)	Cu3–O2	2.667(3)
Cu2–O2	2.000(3)		
Cu2–N2	2.154(3)		
Cu2–N3^{ii}	2.230(3)		

[a] Symmetry codes for **4**: (iii) −0.5 + x, −0.5 − y, −0.5 + z; (iv) −1 + x, y, z; (v) −0.5 − x, 0.5 + y, 2.5 − z. For **5**: (ii) x, 0.5 − y, 0.5 + z; (iv) −x, −0.5 + y, 0.5 − z; (v) 1 + x, y, z.

decreased in view of the generation of two double carboxylate links. This produces only a six-connected cluster/carboxylate subtopology (primitive cubic net), while further cross-linking of the nodes by bipyridazine ligands yields a rarely encountered[33] uninodal ten-coordinated framework with a Schläfli point symbol $\{3^{12}\cdot4^{28}\cdot5^5\}$ (identified by a "**bct**" notation in the Reticular Chemistry Structure Resource database).[34]

Magnetic properties

Compounds 1, 3 and 4, representing the cluster types **A**, **B** and **C**, respectively, were selected for an investigation of their magnetic properties. The $\chi_m T(T)$ plot of a polycrystalline sample of $[Cu_2(\mu\text{-}OH)\{TMA\}(L)(H_2O)]$ (**1**) (scaled per Cu_2 unit) exhibits decreasing $\chi_m T$ values on cooling, starting from 0.91 cm³ K mol⁻¹ at 300 K and approaching a value of 0.05 cm³ K mol⁻¹ at 1.9 K (Fig. 6). This plot is typical of intracluster antiferromagnetic exchange interactions leading to a diamagnetic ground state. This behaviour may be compared with simpler binuclear systems sustained by the mixed hydroxo + *syn–syn* carboxylate bridge between the Cu ions, which exhibit a strong ferromagnetic coupling.[35] The small low temperature $\chi_m T$

Fig. 6 Thermal variation of $\chi_m T$ for **1** (the solid line is drawn based on the Bleaney–Bowers equation).
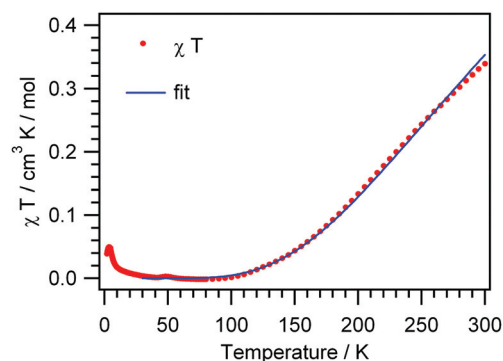
value originates from a minor paramagnetic phase; this is reflected in the Curie tail as seen in the $\chi_m(T)$ plot (Fig. S24†).

The inverse magnetic susceptibility curve (Fig. S25†) shows a linear behavior in the temperature range of 50 to 300 K, which results in a Weiss constant $\theta = -37$ K, in good agreement with the negative slope of the $\chi_m T$ *versus* T curve. We can use the following isotropic Hamiltonian to describe the intracluster magnetic exchange interactions:
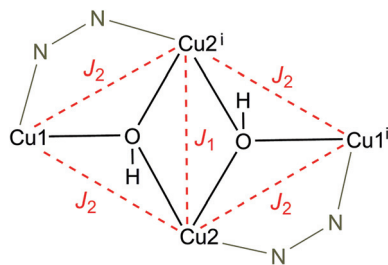
$$H = -2J(S_1 S_2)$$

The magnetic susceptibility data were least-squares fit to the Bleaney–Bowers equation[36] for isotropic exchange in the Cu(II) pair. A good simulation of the data is achieved with $J = -17.5$ cm⁻¹ ($g = 2.1$). The fact that compound **1** shows a very complex bonding pattern with a heteroligand pyridazine/OH/carboxylate triple bridge connecting the two Cu(II) ions prevents a detailed structure–property correlation, and thus the experimentally determined J parameter comprises all possible exchange pathways between the spin centers.

The $\chi_m T(T)$ plot of a polycrystalline sample of $[Cu_4(\mu_3\text{-}OH)_2\{TDC\}_3(L)_2(H_2O)_2]\cdot 7H_2O$ (**3**) (scaled per Cu_4 unit) exhibits strongly decreasing $\chi_m T$ values on cooling, starting from 0.34 cm³ K mol⁻¹ at 300 K and approaching a zero value around 90 K (Fig. 7). The high temperature $\chi_m T$ values are much smaller than the spin-only value of 1.5 cm³ K mol⁻¹ for

Fig. 7 Thermal variation of $\chi_m T$ for **3** (solid line is a fit according to eqn (1)).

Scheme 3 $\{Cu_4(\mu_3\text{-OH})_2\}$ core fragment of **3** and the corresponding magnetic coupling scheme.

four non-interacting spins with $S = 1/2$ ($g = 2.0$) which is due to strong intracluster antiferromagnetic exchange interactions. The low temperature $\chi_m T$ values indicate a diamagnetic ground state of the tetranuclear complex.

Given the butterfly-type arrangement of the tetranuclear cluster fragment (Scheme 3) and leaving aside the asymmetry of the bonding pattern on the wings, we can use it as an approximation which is justified below. The following isotropic Hamiltonian describes the intracluster magnetic exchange interactions [eqn (1)]:

$$H = -2J_1(S_2 S_{2i}) - 2J_2(S_1 S_2 + S_1 S_{2i} + S_2 S_{1i} + S_{2i} S_{1i}) \quad (1)$$

This model approximates the [Cu$_4$] core with a rhombic symmetry while differentiating two magnetic exchange pathways, namely Cu2–Cu2^i (J_1) vs. Cu1–Cu2, Cu1–Cu2^i, Cu2–Cu1^i, Cu2^i–Cu1^i (J_2). Consequently, this Hamiltonian gives rise to six spin states comprising the total spin values (S_T) of 2, 1, 0 with the corresponding energy levels in terms of the magnetic coupling constants as given below:

$$E_1(S_T = 2) = -\frac{1}{2}J_1 - 2J_2$$

$$E_2(S_T = 1) = -\frac{1}{2}J_1 + 2J_2$$

$$E_3(S_T = 1) = -\frac{1}{2}J_1$$

$$E_4(S_T = 1) = +\frac{3}{2}J_1$$

$$E_5(S_T = 0) = -\frac{1}{2}J_1 + 4J_2$$

$$E_6(S_T = 0) = +\frac{3}{2}J_1$$

Applying these energy values to the van Vleck equation gives the following analytical expression [eqn (2)]:
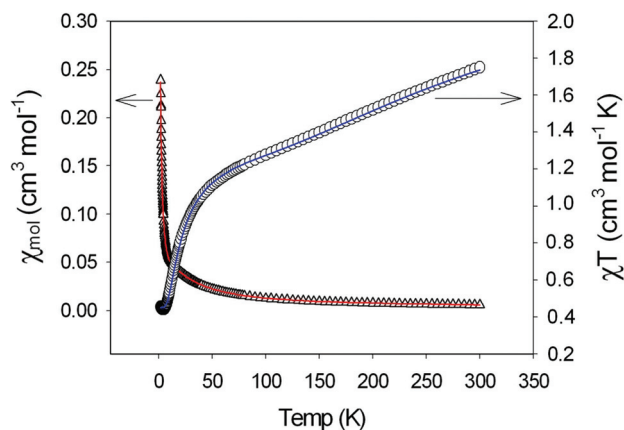
$$\chi_m = 2N\beta^2 g^2/kT(A/B);$$
$$A = 5\exp(-E_1/kT) + \exp(-E_2/kT) + \exp(-E_3/kT)$$
$$\quad + \exp(-E_4/kT) \quad (2)$$
$$B = 5\exp(-E_1/kT) + 3\exp(-E_2/kT) + 3\exp(-E_3/kT)$$
$$\quad + 3\exp(-E_4/kT) + \exp(-E_5/kT) + \exp(-E_6/kT)$$

To reiterate at this stage, the linking pattern at the wing sides of the $\{Cu_4(\mu_3\text{-OH})_2\}$ core differs since on two sides a

chelating pyridazine is involved, a fact which would principally ask for two different exchange parameters, say J_2 and J_3. This would result in six energy levels in the function of three J parameters.[25b] However, in view of the rather smooth curve of the $\chi_m T(T)$ plot one can understand that any trials to fit the data to a three parameter model are not conclusive due to overparametrization. Next, it clearly turned out best to fix the J_1 parameter to a reasonable value of −110 cm^{-1}; this coupling strength results from an analogous core structure[25a] and then using eqn (2), the experimental data were fitted satisfactorily in the temperature range 300–30 K with J_2 = −228 cm^{-1} (g = 2.07). Both values of the coupling constants express the fairly strong antiferromagnetic intracluster coupling which consequently results in a diamagnetic ground state. One has to bear in mind, however, that the J_2 parameter now represents an average coupling value on the wing sides.

The $\chi_m T(T)$ and $\chi_m(T)$ plots of a polycrystalline sample of [Cu$_5$(μ-OH)$_2${BDC}$_4$(L)$_2$(H$_2$O)$_2$]·5H$_2$O (**4**) (scaled per Cu$_5$ unit) are shown in Fig. 8. The high-temperature $\chi_m T$ value of 1.75 cm^3 K mol^{-1} is smaller than the spin-only value of 2.06 cm^3 K mol^{-1} for five non-interacting spins with $S = 1/2$ (g = 2.2) and they decrease to a value approaching zero at 2 K. Both are indicative of strong antiferromagnetic exchange interactions within the pentameric unit.

A structural analysis reveals that the central Cu$_3$ subunit involves Cu1 bound to two equivalent inversion related Cu2 via two bridges, hydroxo and pyridazine. The pyridazine bridges can be considered to be orthogonal connections, because of the short–long bonds to Cu2 and Cu2′ within each pair. Cu–O connections to the bridging OH$^-$ groups are short and since the Cu–OH–Cu angle (114.3°) is large, one would anticipate strong antiferromagnetic exchange between Cu1 and the two Cu2 atoms through these bridges (equatorial–equatorial connections). The Cu2–Cu3 connection is really just a 1,3-carboxylate with short contacts to both copper centers (the aqua O2 donor is just bonded to Cu2 with a short contact, whereas the secondary Cu3–O2 interactions are only very distal and weak, Table 6). Therefore both Cu2 atoms are going to be

Fig. 8 Thermal variation of χ_m and $\chi_m T$ for **4** (the solid lines are a fit to the data).

Table 6 Crystal data for $[Cu_2(\mu\text{-OH})\{TMA\}(L)(H_2O)]$ (**1**), $[Cu_4(\mu_3\text{-OH})_2\{ATC\}_2(L)_2(H_2O)_2]\cdot H_2O$ (**2**), $[Cu_4(\mu_3\text{-OH})_2\{TDC\}_3(L)_2(H_2O)_2]\cdot 7H_2O$ (**3**), $[Cu_5(\mu\text{-OH})_2\{BDC\}_4(L)_2(H_2O)_2]\cdot 5H_2O$ (**4a** and **4b**) and $[Cu_5(\mu\text{-OH})_2\{HO\text{-BDC}\}_4(L)_2(H_2O)_2]\cdot 6H_2O$ (**5**)

	1	2	3	4a	4b	5
Formula	$C_{27}H_{26}Cu_2N_4O_8$	$C_{62}H_{78}Cu_4N_8O_{19}$	$C_{54}H_{66}Cu_4N_8O_{23}S_3$	$C_{68}H_{72}Cu_5N_8O_{25}$	$C_{68}H_{72}Cu_5N_8O_{25}$	$C_{68}H_{74}Cu_5N_8O_{30}$
T, K	213	296	173	296	105	296
M	661.60	1493.48	1545.49	1719.04	1719.04	1801.05
Crystal system	Monoclinic	Triclinic	Monoclinic	Monoclinic	Monoclinic	Monoclinic
Space group, Z	$C2/c$, 8	$P\bar{1}$, 1	$P2_1/n$, 2	$P2_1/n$, 2	$P2_1/n$, 2	$P2_1/c$, 2
$a/\text{Å}$	24.8536(18)	11.1208(9)	13.3933(4)	10.0517(7)	10.0322(6)	10.0552(5)
$b/\text{Å}$	10.8716(7)	11.5078(10)	9.9035(3)	18.4855(9)	18.4439(9)	18.7840(8)
$c/\text{Å}$	18.6837(14)	13.8841(13)	23.7661(8)	19.1143(13)	19.0354(12)	19.1757(9)
α	90	83.981(6)	90	90	90	90
β	101.581(8)	67.507(6)	98.036(2)	104.721(5)	104.897(5)	104.829(2)
γ	90	62.065(5)	90	90	90	90
$V/\text{Å}^3$	4945.5(6)	1444.3(2)	3121.39(17)	3435.1(4)	3403.8(3)	3501.2(3)
$\mu(\text{Mo-K}\alpha)/\text{mm}^{-1}$	1.783	1.541	1.530	1.613	1.627	1.591
$D_c/\text{g cm}^{-3}$	1.777	1.717	1.644	1.662	1.677	1.708
$\theta_{max}/^\circ$	25.96	26.94	27.10	28.54	28.54	27.48
Meas/ Unique reflns	16 964/4789	15 505/6248	29 009/6862	28 251/8582	29 556/8509	31 226/8020
R_{int}	0.041	0.061	0.085	0.042	0.046	0.088
Parameters refined	433	419	477	502	502	502
$R_1 [I > 2\sigma(I)]$	0.033	0.055	0.049	0.036	0.032	0.047
wR_2 [all data]	0.084	0.098	0.104	0.095	0.081	0.104
Goof on F^2	0.917	0.916	0.990	0.965	0.901	1.010
Max, min peak/e Å^{-3}	0.44, −0.78	0.58, −0.59	0.59, −0.51	0.64, −1.10	0.54, −0.55	0.47, −0.53

antiferromagnetically coupled to Cu3, but with a much smaller J value. The corresponding magnetic coupling scheme is given as

$$Cu3\overset{J_2}{\text{—}}Cu2\overset{J_1}{\text{—}}Cu1\overset{J_1}{\text{—}}Cu2^i\overset{J_2}{\text{—}}Cu3^i$$

and the isotropic Hamiltonian is

$$H = -2J_1(S_1S_2 + S_1S_{2i}) - 2J_2(S_2S_3 + S_{2i}S_{3i})$$

The exchange model is therefore based on a strongly antiferromagnetically coupled central linear trinuclear Cu$_3$ group, with the Cu3 centers weakly antiferromagnetically coupled to the terminal coppers (Cu2) of the triad.

In the data fitting J_1 and J_2 were represented as a ratio (J_1/J_2) and after varying the ratio, fitting the data, and observing and minimizing the fitting coefficient, a satisfactory fit was obtained using MAGMUN4.11.[37] This program calculates the total spin states and their energies based on the exchange Hamiltonian, and determines the fitted parameters internally through weighted non-linear least squares procedures. The optimum ratio was found to be $J_1/J_2 = 10$, with the best fit parameters at $J_1 = -125(3)$ cm^{-1}, $J_2 = -12.5(3)$ cm^{-1} and $g = 2.18$, providing the eminently sensible model based on the regression statistics and the structure.

Thermal stability

The thermal behavior of compounds **1–5** was examined by complementary TG/DTA-MS and temperature-dependent powder X-ray diffractometry (TD PXRD) techniques. With the exception of complex **4**, the stages of dehydration and further weight losses due to the thermal destructions are not separated and proceed above 150 °C, with the crystallization of an inorganic product (CuO) observed above 350 °C. Compound **1** is somewhat more stable. It does not show any weight loss

until a temperature of 260 °C. In the range 260–340 °C, with a DTG peak maximum at 300 °C, it decomposes (−29.7%) with dehydration (m/z 18) and release of CO$_2$ (m/z 44) due to decarboxylation. This is accompanied by a loss of crystallinity at 260 °C, as evidenced by PXRD patterns. The stability of the aliphatic analog **2** is comparable. Dehydration starts at 160 °C, and above 220 °C it was accompanied by decarboxylation which results in one unresolved stage of 12.3% weight loss in the range of 160–270 °C (maximum at 250 °C). The PXRD patterns are also indicative of the dehydration process (160–170 °C) since the interlayer spacing is sensitive to elimination of the guest molecules located between the coordination layers. Disintegration of the structure was observed at 230 °C. Complex **3** experiences partial dehydration above 60 °C, with the release of 5 water molecules in the temperature range of 60–170 °C (5.60% observed; 5.82% calculated). This results in a phase transition at 170 °C, and at 195 °C the compound gets amorphous due to decomposition with the release of CO$_2$. For the closely related **4** and **5**, disintegration of the frameworks occurs at an identical temperature of 235 °C. However, due to a more hydrophobic nature of the isophthalate framework in **4**, $vs.$ the 5-hydroxyisophthalate analog **5**, the initial dehydration in the first case proceeds more readily. The TG curve indicates two insufficiently separated stages at 110–200 °C and 200–250 °C, with a total weight loss of 7.3% corresponding to the release of coordinated and outer sphere water molecules (calculated 7.32%). Further thermal decomposition proceeds at 270–340 °C. In the case of **5**, the dehydration begins at 160 °C. Progressive release of water molecules (m/z 18) coincides with beginning of decarboxylation (m/z 44) at 265 °C. The weight loss of 8.5% in the temperature range 160–260 °C corresponds to the elimination of 8 water molecules (calculated 8.0%).

IR spectra

The IR spectra of complexes **1–5** exhibit strong and broad absorption bands in the region of 3230–3500 cm^{-1}, which are attributed to the ν(OH) vibrations of the aqua and hydroxo ligands. Bands at 2850–2933 cm^{-1} correspond to ν(CH) vibrations of adamantane and aromatic moieties. The absorptions for the carbonyl group, ν(CO), appear as very strong bands at 1590–1627 cm^{-1} (see the Experimental section). The absence of bands at 1730–1690 cm^{-1}, where ν(CO) of COOH is expected to appear, confirms full deprotonation of the polycarboxylate ligands in **1–5**.[38] Strong absorption bands at 1358–1382 cm^{-1} are characteristic of all the compounds; they could be assigned to ν(CN) of the pyridazine rings.[39]

Conclusions

The present results are important for providing innovative strategies for the construction of extended coordination lattices incorporating polynuclear metal–organic clusters. A combination of pyridazine, carboxylate and hydroxo ligands is especially well suited for sustaining coordination patterns of different nuclearities and connectivities: this kind of bridges reveals a perfect compatibility and they readily complement each other and act in a synergistic manner. In cooperation with μ-carboxylate and, especially μ-hydroxo groups, pyridazine typically behaves as a short-distance diatomic bridge. Therefore, the present heteroligand system unites and extends the structural and functional potential of such common types of organic and inorganic bridges for the generation of discrete polynuclear arrangements of metal ions. At the same time, a multiplication of the ligand functionality, as it occurs for di- and tricarboxylate and bipyridazine ligands, allows the integration of the clusters into polymeric arrays, which could be anticipated for a broad range of transition metal ions and different kinds of organic linkers. Our study suggests also a new approach and attractive preparative sequence towards bridge-head heteroaryl C-functionalization of adamantane, which could find wider applications for the development of multivalent geometrically rigid molecular building blocks incorporating "nanodiamond scaffolds".[40] Moreover, the study of magnetic properties of coordination network compounds is a very topical issue in the field of molecular magnetism.[41] In the present case, the magnetic susceptibility data for clusters **1**, **3** and **4** reveal substantial antiferromagnetic coupling strengths, however, with varying ratios of the coupling parameters. In particular, common to all three structure types **A**, **B** and **C** is the quite complex nature of bonding patterns including heteroligand multiple bridges connecting the spin centers, which prevents a discussion of more detailed structure–property correlations.

Experimental

All starting materials were chemicals of reagent grade and used as received without further purification. Adamantane-

1,3,5-tricarboxylic acid was synthesized in 62% yield by the Koch–Haaf carboxylation of 1,3,5-adamantanetriol with 100% HCOOH in a 15% oleum medium.[42] The 1,2,4,5-tetrazine was prepared and freshly purified by sublimation as described previously.[13,14c]

Synthesis of 1,3-bis(pyridazin-4-yl)adamantane (L) (Scheme 1). A solution of 1.24 g (15.1 mmol) 1,2,4,5-tetrazine and 1.26 g (6.8 mmol) 1,3-diethynyladamantane[43] in 40 ml of dry 1,4-dioxane was stirred at 90 °C over a period of 25 h. The reaction proceeded smoothly and the evolution of dinitrogen gas ceased after 15–16 h. The precipitate was filtered off, washed with 1,4-dioxane and diethyl ether and dried in air. It was dissolved in boiling methanol and the solution was decolorized by 15 min reflux with charcoal, then it was filtered and evaporated yielding 1.41 g (71%) of a colorless crystalline product. ^{1}H NMR (400 MHz, dmso-d$_6$): δ 9.38–9.28 (m, 2H), 9.06 (d, J = 5.4 Hz, 2H), 7.58 (dd, J = 5.5, 2.6 Hz, 2H), 2.42–2.32 (m, 2H), 2.10 (s, 2H), 1.98 (t, J = 3.7 Hz, 8H), 1.82 (d, J = 3.5 Hz, 2H). Anal. Calcd for C$_{18}$H$_{20}$N$_4$: C, 73.94; H, 6.90; N, 19.17. Found: C, 74.06; H, 6.88; N, 19.04.

Preparation of the coordination compounds

The complexes were prepared under hydrothermal conditions as follows. A mixture of the starting compounds and distilled water were placed in a 20 mL Teflon-lined stainless steel autoclave, stirred for 10–30 min, and heated at 140 °C for 40–70 h in an oven, with further cooling to room temperature. In each case, the excess of bipyridazine ligand was essential for partial hydrolysis of Cu(II) ions and generation of the desired hydroxo-bridged species. Under these conditions and absence of di- or tricarboxylate components, the reactions of Cu(OAc)$_2$·H$_2$O and the bipyridazine ligand did not afford insoluble products.

Synthesis of [Cu$_2$(μ-OH){TMA}(L)(H$_2$O)] (1). A mixture of 6.8 mg (0.034 mmol) Cu(OAc)$_2$·H$_2$O, 3.1 mg (0.015 mmol) trimesic acid and 10.0 mg (0.034 mmol) ligand in a 1 : 0.44 : 1 molar ratio with 4 mL water was stirred for 30 min in a Teflon vessel, and then it was heated at 140 °C for 70 h. Slow cooling to r.t. over a period of 48 h (cooling rate 2.5 °C h^{-1}) afforded a pure product as green prisms, which were washed with 3 mL of water and dried in air for 1 h (yield: 7.9 mg, 80%). Anal. Calcd for C$_{27}$H$_{26}$Cu$_2$N$_4$O$_8$: C, 49.01; H, 3.96; N, 8.47. Found: C, 48.89; H, 4.01; N, 8.35. IR (KBr discs, selected bands, cm^{-1}): 568w, 717s, 761m, 977w, 1022w, 1091w, 1359vs, 1407m, 1433s, 1558vs, 1607vs, 2852w, 2900m, 3233mbr, 3409m.

Synthesis of [Cu$_4$(μ$_3$-OH)$_2${ATC}$_2$(L)$_2$(H$_2$O)$_2$]·H$_2$O (2). The compound was prepared in a similar manner, starting with 6.8 mg (0.034 mmol) Cu(OAc)$_2$·H$_2$O, 3.5 mg (0.013 mmol) adamantane-1,3,5-tricarboxylic acid, 10.0 mg (0.034 mmol) ligand (1 : 0.38 : 1 molar ratio) and 4 mL of water. Small green prismatic crystals of the product were obtained in 80% yield. Anal. Calcd for C$_{62}$H$_{78}$Cu$_4$N$_8$O$_{19}$: C, 49.86; H, 5.26; N, 7.50. Found: C, 50.03; H, 5.19; N, 7.59. IR (KBr discs, selected bands, cm^{-1}): 568w, 710m, 832w, 1084w, 1209w, 1274m, 1328s, 1358vs, 1442w, 1590vs, 2850m, 2930s, 3044m, 3269mbr, 3471mbr.

Synthesis of $[Cu_4(\mu_3\text{-}OH)_2\{TDC\}_3(L)_2(H_2O)_2]\cdot 7H_2O$ (3). An equimolar mixture of 5.0 mg (0.025 mmol) $Cu(OAc)_2\cdot H_2O$, 4.3 mg (0.025 mmol) 2,5-thiophenedicarboxylic acid, 7.4 mg (0.025 mmol) ligand were placed in a Teflon vessel, and 5 mL of water was added. The mixture was stirred for 30 min and then it was heated at 140 °C for 24 h. Small blue prisms of the pure product were obtained in 60% yield after slow cooling to r.t. for a period of 72 h. Anal. Calcd for $C_{54}H_{66}Cu_4N_8O_{23}S_3$: C, 41.96; H, 4.30; N, 7.25. Found: C, 42.11; H, 4.22; N, 7.37. IR (KBr discs, selected bands, cm^{-1}): 556w, 689w, 774m, 808w, 973w, 1022w, 1072w, 1111w, 1314s, 1358vs, 1452w, 1527s, 1561s, 1597vs, 2852m, 2913m, 3407sbr.

Synthesis of $[Cu_5(\mu\text{-}OH)_2\{BDC\}_4(L)_2(H_2O)_2]\cdot 5H_2O$ (4). A mixture of 6.8 mg (0.034 mmol) $Cu(OAc)_2\cdot H_2O$, 5.7 mg (0.034 mmol) isophthalic acid, 10.0 mg (0.034 mmol) ligand, all in an equimolar ratio, and 4 mL of water was stirred for 10 min and then heated at 140 °C for 24 h in a Teflon vessel. After cooling to r.t. for a period of 72 h, large blue-green crystals of the pure product were collected by filtration (yield: 9.3 mg, or 80%, based on Cu). Anal. Calcd for $C_{68}H_{72}Cu_5N_8O_{25}$: C, 47.51; H, 4.22; N, 6.52. Found: C, 47.59; H, 4.19; N, 6.63. IR (KBr discs, selected bands, cm^{-1}): 548w, 716m, 748m, 806w, 1084w, 1156w, 1268w, 1368s, 1390vs, 1450m, 1476w, 1560s, 1622vs, 2856m, 2922m, 3400sbr, 3456sbr.

Synthesis of $[Cu_5(\mu\text{-}OH)_2\{HO\text{-}BDC\}_4(L)_2(H_2O)_2]\cdot 6H_2O$ (5). The compound was prepared similarly as for **4** from a mixture of 6.8 mg (0.034 mmol) $Cu(OAc)_2\cdot H_2O$, 6.2 mg (0.034 mmol) 5-hydroxyisophthalic acid and 10.0 mg (0.034 mmol) ligand, giving large blue-green prisms (yield 75%). Anal. Calcd for $C_{68}H_{74}Cu_5N_8O_{30}$: C, 45.34; H, 4.14; N, 6.22. Found: C, 45.47; H, 4.13; N, 6.39. IR (KBr discs, selected bands, cm^{-1}): 558w, 646w, 678w, 721s, 777s, 985m, 1001m, 1021m, 1102w, 1128w, 1195m, 1218w, 1265m, 1280m, 1296m, 1382vs, 1420s, 1449m, 1472m, 1545s, 1593s, 1627s, 2856m, 2899m, 2933s, 3370sbr, 3500s, 3586m.

Measurements

Thermogravimetric/differential thermal analysis mass spectrometry (TG/DTA-MS) was performed on a Netzsch F1 Jupiter device connected to an Aeolos mass spectrometer. The sample was heated at a rate of 10° min^{-1}. The temperature-dependent X-ray measurements were carried out on a Stoe STADIP with a high-temperature attachment and a image-plate detector system. PXRD was carried out on a Stoe STADIP (Cu K$_{\alpha1}$) using a linear PSD detector and on a Shimadzu XRD-6000 (Cu Kα radiation). Elemental analysis was carried out with a Vario EL-Heraeus microanalyzer. IR spectra (400–4000 cm^{-1}, KBr disks) were collected using a Perkin-Elmer FTIR spectrometer.

Magnetic susceptibility measurements were made on a Quantum Design MPMS SQUID-*XL* magnetometer under an applied magnetic field of 10^3 Oe between 300 and 1.9 K. The samples were prepared in a gelatine capsule. Diamagnetic corrections were made for the samples using the approximation $-0.45 \times$ molecular weight $\times 10^{-6}$ cm^3 mol^{-1} and the sample holder was corrected for by measuring directly the susceptibility of the empty capsule.

X-Ray crystallography

The diffraction data were collected with graphite-monochromated Mo-Kα radiation (λ = 0.71073 Å) (Table 6). Measurements for **1** at 213 K and for **4** (**4a**: 296 K, **4b**: 105 K) were made using a Stoe Image Plate Diffraction System, φ oscillation scans (numerical absorption correction using X-RED and X-SHAPE).[44] Measurements for **2**, **3** and **5** were performed at 173 K on a Bruker APEXII CCD area-detector diffractometer (ω scans). The data were corrected for Lorentz-polarization effects and for the effects of absorption (multi-scans method). The structures were solved by direct methods and refined by full-matrix least-squares on F^2 using the SHELX-97 package.[45] The CH-hydrogen atoms were added geometrically, with U_{iso} = $1.2U_{eq}$ (C) and OH-hydrogen atoms were located and included with fixed d (O–H) = 0.85 Å and U_{iso} = $1.5U_{eq}$ (O). Part of the solvate water molecules in **2–4** is disordered. They were refined anisotropically and the hydrogen atoms were not added. In **1**, the binuclear cluster is equally disordered over two positions (Cu ion, μ-OH and aqua ligand; one of the pyridazine cycles is also disordered adopting two orientations). Attempted refinements in space groups of lower symmetry did not afford an ordered model. This fragment was freely refined anisotropically and the hydrogen atoms were added as stated above with partial contributions of 0.5. In **3**, one of the TDC^{2-} ligands is equally disordered over two positions across a center of inversion. The disorder was resolved without restraints in geometry, but with restrained parameters for thermal motion of the carbon atoms. The topological analysis was performed using TOPOS 4.0[46] and Graphical visualization of the structures was made using the program Diamond 2.1e.[47]

References

1 D. J. Tranchemontagne, J. L. Mendoza-Cortés, M. O'Keeffe and O. M. Yaghi, *Chem. Soc. Rev.*, 2009, **38**, 1257; J. J. Perry IV, J. A. Perman and M. J. Zaworotko, *Chem. Soc. Rev.*, 2009, **38**, 1400; H. Furukawa, N. Ko, Y. B. Go, N. Aratani, S. B. Choi, E. Choi, A. O. Yazaydin, R. Q. Snurr, M. O'Keeffe, J. Kim and O. M. Yaghi, *Science*, 2010, **329**, 424; J. Kim, B. Chen, T. M. Reineke, H. Li, M. Eddaoudi, D. B. Moler, M. O'Keeffe and O. M. Yaghi, *J. Am. Chem. Soc.*, 2001, **123**, 8239.

2 M. O'Keeffe, M. A. Peskov, S. J. Ramsden and O. M. Yaghi, *Acc. Chem. Res.*, 2008, **41**, 1782.

3 P. Hubberstey, X. Lin, N. R. Champness and M. Schröder, in *Metal-Organic Frameworks: Design and Applications*, John Wiley & Sons, Inc., Hoboken, New Jersey, 2010.

4 Q. Lin, T. Wu, X. Bu and P. Feng, *Dalton Trans.*, 2012, **41**, 3620; J. Jia, X. Lin, C. Wilson, A. J. Blake, N. R. Champness, P. Hubberstey, G. Walker, E. J. Cussen and M. Schröder, *Chem. Commun.*, 2007, 840; G.-H. Cui, C.-H. He, C.-J. Jiao, J.-C. Geng and V. A. Blatov, *CrystEngComm*, 2012, **14**, 4210; X.-M. Zhang, R.-Q. Fang and H.-S. Wu, *J. Am. Chem. Soc.*, 2005, **127**, 7670; D. Li, T. Wu, X.-P. Zhou, R. Zhou and X.-C. Huang, *Angew. Chem., Int. Ed.*, 2005, **44**, 4175; J. H. Cavka, S. Jakobsen, U. Olsbye, N. Guillou, C. Lamberti, S. Bordiga and K. P. Lillerud, *J. Am. Chem. Soc.*, 2008, **130**, 13850.

5 C. Janiak, *Dalton Trans.*, 2003, 2781.

6 C. Heering, I. Boldog, V. Vasylyeva, J. Sanchiz and C. Janiak, *CrystEngComm*, 2013, **15**, 9757.

7 B. Gil-Hernández, P. Gili, J. K. Vieth, C. Janiak and J. Sanchiz, *Inorg. Chem.*, 2010, **49**, 7478; J. K. Maclaren, J. Sanchiz, P. Gilib and C. Janiak, *New J. Chem.*, 2012, **36**, 1596; H. H. Monfared, J. Sanchiz, Z. Kalantari and C. Janiak, *Inorg. Chim. Acta*, 2009, **362**, 3791.

8 F. A. Almeida Paz, J. Klinowski, S. M. F. Vilela, J. P. C. Tomé, J. A. S. Cavaleiro and J. Rocha, *Chem. Soc. Rev.*, 2012, **41**, 1088; D. Zhao, D. J. Timmons, D. Yuan and H.-C. Zhou, *Acc. Chem. Res.*, 2011, **44**, 123.

9 S. S. Tandon, L. K. Thompson and R. C. Hynes, *Inorg. Chem.*, 1992, **31**, 2210; C. Li, N. Kanehisa, Y. Miyagi, Y. Nakao, S. Takamizawa, W. Mori and Y. Kai, *Bull. Chem. Soc. Jpn.*, 1997, **70**, 2429.

10 T. Yi, C. Ho-Chol, S. Gao and S. Kitagawa, *Eur. J. Inorg. Chem.*, 2006, 1381.

11 A.-C. Knall and C. Slugovc, *Chem. Soc. Rev.*, 2013, **42**, 5131.

12 A. T. M. Marcelis and H. C. van der Plas, *J. Heterocycl. Chem.*, 1987, **24**, 545; J. Sauer, D. K. Heldmann, J. Hetzenegger, J. Krauthan, H. Sichert and J. Schuster, *Eur. J. Org. Chem.*, 1998, 2885.

13 K. V. Domasevitch, I. A. Gural'skiy, P. V. Solntsev, E. B. Rusanov, H. Krautscheid, J. A. K. Howard and A. N. Chernega, *Dalton Trans.*, 2007, 3140.

14 (a) I. A. Gural'skiy, P. V. Solntsev, H. Krautscheid and K. V. Domasevitch, *Chem. Commun.*, 2006, 4808; (b) K. V. Domasevitch, P. V. Solntsev, I. A. Gural'skiy, H. Krautscheid, E. B. Rusanov, A. N. Chernega and J. A. K. Howard, *Dalton Trans.*, 2007, 3893; (c) A. S. Degtyarenko, P. V. Solntsev, H. Krautscheid, E. B. Rusanov, A. N. Chernega and K. V. Domasevitch, *New J. Chem.*, 2008, **32**, 1910.

15 T. Otieno, S. J. Rettig, R. C. Thompson and J. Trotter, *Inorg. Chem.*, 1995, **34**, 1718.

16 K. V. Domasevitch, J. A. Rusanova, I. A. Gural'skiy and P. V. Solntsev, *Acta Crystallogr., Sect. C: Cryst. Struct. Commun.*, 2012, **68**, m295.

17 C. Näther and I. Jeß, *Inorg. Chem.*, 2003, **42**, 2968; P. V. Solntsev, J. Sieler, H. Krautscheid and K. V. Domasevitch, *Dalton Trans.*, 2004, 1153; K. V. Domasevitch, P. V. Solntsev, H. Krautscheid, I. S. Zhylenko, E. B. Rusanov and A. N. Chernega, *Chem. Commun.*, 2012, **48**, 5847; L. Plasseraud, H. Maid, F. Hampel and R. W. Saalfrank, *Chem. – Eur. J.*, 2001, **7**,

4007; A. S. Batsanov, M. Begley, M. W. George, P. Hubberstey, M. Munakata, C. Russell and P. H. Walton, *J. Chem. Soc., Dalton Trans.*, 1999, 4251; M. Maekawa, M. Munakata, T. Kuroda-Sowa and Y. Nozaka, *J. Chem. Soc., Dalton Trans.*, 1994, 603; M. J. Begley, P. Hubberstey, C. E. Russell and P. H. Walton, *J. Chem. Soc., Dalton Trans.*, 1994, 2483; D. Hagrman, C. Sangregorio, C. J. O'Connor and J. Zubieta, *J. Chem. Soc., Dalton Trans.*, 1998, 3707.

18 F. Lloret, G. De Munno, M. Julve, J. Cano, R. Ruiz and A. Caneschi, *Angew. Chem., Int. Ed.*, 1998, **37**, 135; A. Escuer, F. A. Mautner, N. Sanz and R. Vicente, *Inorg. Chim. Acta*, 2002, **340**, 163; T. Otieno, S. J. Rettig, R. C. Thompson and J. Trotter, *Acta Crystallogr., Sect. C: Cryst. Struct. Commun.*, 1993, **49**, 2067; L. Pazderski, E. Szlyk, A. Wojtczak, L. Kozerski and J. Sitkowski, *Acta Crystallogr., Sect. E: Struct. Rep. Online*, 2004, **60**, 1270; E. Krupicka and A. Lentz, *Z. Kristallogr. - New Cryst. Struct.*, 2001, **216**, 289; A. S. Degtyarenko and K. V. Domasevitch, *Acta Crystallogr., Sect. C: Cryst. Struct. Commun.*, 2013, **69**, 219.

19 L. Carlucci, G. Ciani, M. Moret and A. Sironi, *J. Chem. Soc., Dalton Trans.*, 1994, 2397.

20 (a) T. Fetzer, A. Lentz, T. Debaerdemaeker and O. Abou-El-Wafa, *Z. Naturforsch., Teil B*, 1990, **45**, 199; (b) L. Pazderski, E. Szlyk, A. Wojtczak, L. Kozerski, J. Sitkowski and B. Kamieński, *J. Mol. Struct.*, 2004, **697**, 143.

21 J. Cano, G. De Munno, F. Lloret and M. Julve, *Inorg. Chem.*, 2000, **39**, 1611.

22 T. V. Yilmaz, E. Senel and C. Kazak, *Aust. J. Chem.*, 2008, **61**, 634.

23 K. Hyde, G. F. Kokoszka and G. Gordon, *J. Inorg. Nucl. Chem.*, 1969, **31**, 1993; J. R. Ferraro, J. Zipper and W. Wozniak, *Appl. Spectrosc.*, 1969, **23**, 160; J. R. Allan, G. A. Barnes and D. H. Brown, *J. Inorg. Nucl. Chem.*, 1971, **33**, 3765; S. Emori, M. Inoue and M. Kubo, *Bull. Chem. Soc. Jpn.*, 1972, **45**, 2259.

24 C. B. Aakeröy, N. R. Champness and C. Janiak, *CrystEng-Comm*, 2010, **12**, 22; B. Wisser, Y. Lu and C. Janiak, *Z. Anorg. Allg. Chem.*, 2007, **633**, 1189; H. A. Habib, A. Hoffmann, H. A. Höppe and C. Janiak, *Dalton Trans.*, 2009, 1742; H. A. Habib, J. Sanchiz and C. Janiak, *Dalton Trans.*, 2008, 1734.

25 (a) G. A. Senchyk, A. B. Lysenko, H. Krautscheid, E. B. Rusanov, A. N. Chernega, K. W. Krämer, S.-X. Liu, S. Decurtins and K. V. Domasevitch, *Inorg. Chem.*, 2013, **52**, 863; (b) H. A. Habib, J. Sanchiz and C. Janiak, *Inorg. Chim. Acta*, 2009, **362**, 2452; (c) G. A. Senchyk, A. B. Lysenko, H. Krautscheid, J. Sieler and K. V. Domasevitch, *Acta Crystallogr., Sect. C: Cryst. Struct. Commun.*, 2008, **64**, m246.

26 A. W. Addison, T. N. Rao, J. Reedijk, J. van Rijn and G. C. Verschoor, *J. Chem. Soc., Dalton Trans.*, 1984, 1349.

27 V. A. Blatov, L. Carlucci, G. Ciani and D. M. Proserpio, *CrystEngComm*, 2004, **6**, 378.

28 I. A. Baburin, V. A. Blatov, L. Carlucci, G. Ciani and D. M. Proserpio, *J. Solid State Chem.*, 2005, **178**, 2452; I. A. Baburin, V. A. Blatov, L. Carlucci, G. Ciani and D. M. Proserpio, *CrystEngComm*, 2008, **10**, 1822;

I. A. Baburin, V. A. Blatov, L. Carlucci, G. Ciani and D. M. Proserpio, *Cryst. Growth Des.*, 2008, **8**, 519.

29 S. S. Chui, S. M. Lo, J. P. Charmant, A. G. Orpen and I. D. Williams, *Science*, 1999, **283**, 1148; L. Alaerts, E. Séguin, H. Poelman, F. Thibault-Starzyk, P. A. Jacobs and D. E. D. Vos, *Chem. – Eur. J.*, 2006, **12**, 7353.

30 G.-X. Liu, K. Zhu, H. Chen, R.-Y. Huang, H. Xu and X.-M. Ren, *Inorg. Chim. Acta*, 2009, **362**, 1605; K.-H. He, Y.-W. Li, Y.-Q. Chen, W.-C. Song and X.-H. Bu, *Cryst. Growth Des.*, 2012, **12**, 2730; H. Li, W. Shi, K. Zhao, Zh. Niu, H. Li and P. Cheng, *Chem. – Eur. J.*, 2013, **19**, 3358; H.-H. Li, W. Shi, N. Xu, Zh.-J. Zhang, Zh. Niu, T. Han and P. Cheng, *Cryst. Growth Des.*, 2012, **12**, 2602.

31 M. A. Halcrow, *Dalton Trans.*, 2003, 4375; M. A. Halcrow, *Chem. Soc. Rev.*, 2013, **42**, 1784.

32 L. R. Falvello, *J. Chem. Soc., Dalton Trans.*, 1997, 4463; J. D. Dunitz, V. Schomaker and K. N. Trueblood, *J. Phys. Chem.*, 1988, **92**, 856.

33 W.-C. Song, Q. Pan, P.-C. Song, Q. Zhao, Y.-F. Zeng, T.-L. Hu and X.-H. Bu, *Chem. Commun.*, 2010, **46**, 4890.

34 (*a*) Reticular Chemistry Structure Resource (RCSR), http://rcsr.anu.edu.au; (*b*) V. A. Blatov and A. P. Shevchenko, *TOPOS 4.0*, Samara State University, Russia, 1999.

35 H. A. Habib, J. Sanchiz and C. Janiak, *Dalton Trans.*, 2008, 4877.

36 B. Bleaney and K. D. Bowers, *Proc. R. Soc. London, Ser. A*, 1952, **214**, 451.

37 MAGMUN4.11/OW01.exe is available as a combined package free of charge from the authors (http://www.ucs.mun.ca/~lthomp/magmun). MAGMUN was developed by Dr Zh. Xu (Memorial University), and OW01.exe by Dr O. Waldmann.

38 W. Brzyska and P. Sadowski, *Pol. J. Chem.*, 1987, **61**, 273; W. Brzyska and W. Wolodkiewicz, *Pol. J. Chem.*, 1986, **60**,

697; K. Wieghardt, *J. Chem. Soc., Dalton Trans.*, 1973, 2548; L. J. Bellamy, *The Infrared Spectra of Complex Molecules*, Wiley, New York, 1958.

39 S. Breda, I. D. Reva, L. Lapinski, M. J. Nowak and R. Fausto, *J. Mol. Struct.*, 2006, **786**, 193; J. Vázquez, J. J. L. Gozález, F. Márquez and J. E. Boggs, *J. Raman Spectrosc.*, 1998, **29**, 547.

40 M. A. Gunawan, J.-C. Hierso, D. Poinsot, A. A. Fokin, N. A. Fokina, B. A. Tkachenko and P. R. Schreiner, *New. J. Chem.*, 2014, **38**, 28.

41 (*a*) O. Kahn, *Molecular Magnetism*, VCH, Weinheim, Gemany, 1993; (*b*) L. K. Thompson (ed.) *Magnetism: Molecular and Supramolecular Perspectives*, *Coord. Chem. Rev.*, 2005, **249**, 2549 (*c*) F. Bonadiao, M.-C. Senna, J. Ensling, A. Sieber, A. Neels, H. Stoeckli-Evans and S. Decurtins, *Inorg. Chem.*, 2005, **44**, 969; (*d*) M. Pilkington and S. Decurtins, *Chimia*, 2000, **54**, 593.

42 G. A. Senchyk, A. B. Lysenko, I. Boldog, E. B. Rusanov, A. N. Chernega, H. Krautscheid and K. V. Domasevitch, *Dalton Trans.*, 2012, **41**, 8675.

43 T. G. Archibald, A. A. Malik and K. Baum, *Macromolecules*, 1991, **24**, 5261.

44 (*a*) *Stoe & Cie, X-SHAPE, Revision 1.06*, Stoe & Cie GmbH, Darmstadt, Germany, 1999; (*b*) *Stoe & Cie, X-RED, Version 1.22*, Stoe & Cie GmbH, Darmstadt, Germany, 2001.

45 G. M. Sheldrick, *Acta Crystallogr., Sect. A: Found. Crystallogr.*, 1990, **46**, 467; G. M. Sheldrick, *Acta Crystallogr., Sect. A: Found. Crystallogr.*, 2008, **64**, 112.

46 V. A. Blatov, TOPOS, IUCr CompComm Newsletter, 2006, 7, 4; V. A. Blatov, A. P. Shevchenko and V. N. Serezhkin, *J. Appl. Crystallogr.*, 2000, **33**, 1193.

47 K. Brandenburg, *Diamond 2.1e*, Crystal Impact GbR, Bonn, 1999.